Laser and Particle Beams (2000), *18*, 623–638. Printed in the USA.

MHD simulations of plasma dynamics in pinch discharges in capillary plasmas

N.A. BOBROVA,[1] S.V. BULANOV,[2] D. FARINA,[3] R. POZZOLI,[3,4] T.L. RAZINKOVA,[1] J.I. SAKAI,[5] P.V. SASOROV,[1] AND I.V. SOKOLOV[2]

[1]Institute for Theoretical and Experimental Physics, B. Cheremushkinskaya str. 25, 117259 Moscow, Russia
[2]General Physics Institute of the Russian Academy of Sciences, Vavilov str. 38, 117942 Moscow, Russia
[3]Istituto di Fisica del Plasma, Consiglio Nazionale delle Ricerche, via Roberto Cozzi 53, 20125 Milano, Italia
[4]Dipartimento di Fisica, Universita di Milano, via Celoria 16, 20133 Milano, Italia
[5]Laboratory for Plasma Astrophysics,Faculty of Engineering, Toyama University, 3190, Gofuku, Toyama, 930 Japan

(RECEIVED 10 November 1999; ACCEPTED 19 June 2000)

Abstract

Magnetohydrodynamic simulation results related to the capillary discharge dynamics are presented. The main physical process that should be taken into account is the ablation of the capillary wall material evaporated by the heat flux from the capillary plasma. The possible applications of the capillary discharges related to the physics of the X-ray lasers and the use of the capillary plasma to provide a guiding for ultrashort high-intensity laser pulses over a distance greater than the defocusing length are discussed.

1. INTRODUCTION

A principal scheme of capillary discharge is extremely simple. The base element is a narrow channel (the radius and the length are on the order of 10^{-2} cm and 10 cm, respectively) made in a solid insulator material. The channel is ended in a longitudinal direction by the two electrodes. An external low-inductance forming line is used to apply a voltage between the electrodes and to form a short pulse (with a typical duration on the order of 100 ns) of the electric current through the cross section of the channel. The electric current heats both the channel wall material and the plasma inside the channel and its magnetic field causes plasma pinching. Capillary discharges were originally studied in nuclear fusion researches (Fisher *et al*., 1973; McCorkle, 1983; Sethian *et al.*, 1985). They may also be used as an intense source of the continuum and line emission for the spectroscopy applications as well as for soft-X-ray microscopy and lithography (Bogen *et al.*, 1968; McCorkle, 1981).

In this article we present the results of magnetohydrodynamic (MHD) simulations of capillary discharge dynamics. We also discuss two possible applications of capillary discharges related to the physics of X-ray lasers and to the use of capillary plasma as a waveguide for ultrashort high-intensity laser pulses, which allows us to provide a pulse guiding over a distance greater than the defocusing length.

One of the most important applications of capillary discharges is relevant to the production of the active media for the X-ray lasers. It is well known that for short-wavelength laser action it is necessary to produce a highly ionized dense plasma filament. The direct generation of an amplifying plasma column by a fast discharge through a capillary channel has been successfully used for the production of highly ionized plasmas with the parameters that are suitable for soft-X-ray lasers (Steden & Kunze, 1990; Rocca *et al.*, 1993, 1994*a*, 1994*b*, 1995, 1996; Tomasel *et al.*, 1993; Kunze *et al.*, 1994; Morgan *et al.*, 1994, 1995; Shin *et al.*, 1994; Hosokai *et al.*, 1997; Benware *et al.*, 1998; Moreno *et al.*, 1998, 1999; Rocca, 1999). This approach has obvious advantages, resulting in the development of compact, efficient, and simple soft-X-ray lasers.

The experiments reported are of two types. In the first type, the capillary discharge is used to generate plasma in a channel filled with an initially preionized gas (Rocca *et al.*, 1994*a*, 1996; Hosokai *et al.*, 1997). In the second one, a plasma is created from a discharge by ionizing the material ablated from the capillary walls (Steden & Kunze, 1990; Tomasel *et al.*, 1993; Morgan *et al.*, 1994; Shin *et al.*, 1994). The mechanism responsible for the amplified spontaneous emission in a capillary filled with argon is electron-collisional excitation pumping of $3p$–$3s$ transition in Ne-like Ar (Rocca *et al.*, 1994*a*). The X-ray laser scheme in evacuated cap-

Address correspondence and reprint requests to: I.V. Sokolov, Laboratory of Plasma Astrophysics, Toyama University, Gofku 3190, Toyama, Japan. E-mail: sokolov@ecs.tomyama-u.ac.jp

illaries involves the population inversion by the enhanced recombination of dense plasmas (Steden & Kunze, 1990). On highly ionizing, the plasma cools rapidly by conductive losses to the capillary walls and then recombines in a three-body recombination process. A particular transition of interest is the C VI H_α ($n = 2$–3) line at 18.2 nm (from H-like C^{5+} ions) for which the amplification is observed in a capillary-discharge plasma (Steden & Kunze, 1990; Shin *et al.*, 1994).

The second application of capillary plasmas is related to the question of how one can provide a guiding for ultrashort high-intensity laser pulses over a distance greater than the defocusing length. Ultrashort laser pulses with an intensity as high as $10^{18–22}$ W/cm^2 provide a broad range of applications (Joshi & Corkum, 1995) that include high harmonic generation, X-ray lasers, nuclear fusion, and charged particle acceleration (Tajima & Dawson, 1979; Modena *et al.*, 1995; Nakajima *et al.*, 1995; Katsouleas & Bingham, 1996). In most applications, the conditions should be created for both the sharp focusing of laser radiation to a small spot of a radius r_0 and the transportation of the pulse over many Rayleigh lengths without diffraction spreading, which are realized, in general, in different limits of laser pulse and plasma parameters.

In the case of the Laser Wake Field Accelerator (Tajima & Dawson, 1979; Gorbunov & Kirsanov, 1987; Sprangle *et al.*, 1988; Esarey *et al.*, 1993; Katsouleas & Bingham, 1996) one should provide laser pulse transportation through the underdense plasma over a distance on the order of the acceleration length, $l_{acc} \approx (c/\omega_{pe})(\omega_0/\omega_{pe})^2$, without significant spreading. Here $\omega_{pe} = (4\pi n_e e^2/m)^{1/2}$ is the Langmuir frequency, and ω_0 is the carrier frequency of laser radiation. The ratio $\omega_0/\omega_{pe} \propto n_e^{-1/2}$, where n_e is the electron plasma density, is supposed to be as large as $\omega_0/\omega_{pe} \approx 10$–100. However, this ratio cannot be too large if one needs to get into a regime with a fairly high rate of charged particle acceleration, since the electric-field amplitude in the wake wave is proportional to $n_e^{1/2}$. In addition, in order for the particles not to slip out of the acceleration phase in the model of unlimited wake-field acceleration, which can be realized in a nonuniform plasma with a properly chosen density profile (Bulanov *et al.*, 1993, 1997*a*), the laser pulse should be guided over distances larger than l_{acc}.

To achieve the regime of laser pulse transportation without diffraction spreading, one invokes either the self-focusing of the high-power electromagnetic radiation in an underdense plasma (Max *et al.*, 1974; Sun *et al.*, 1987; Borisov *et al.*, 1992; Dufree & Milchberg, 1993) or the pulse is supposed to be guided inside the initially performed hollow or inside a narrow channel prefilled with a plasma (Tajima, 1985; Sprangle *et al.*, 1990; Bulanov *et al.*, 1994; Chou *et al.*, 1995; Dufree *et al.*, 1995). The possibility of a laser pulse guiding resulting from relativistic self-focusing, and the electron acceleration in a relativistically self-guided channel were demonstrated by Borisov *et al.* (1992), Dufree and Milchberg (1993), and Wagner *et al.* (1997). This regime is realized only with laser light intensities greater than $P_{crit} \approx 16.5 (\omega_0/\omega_{pe})^2$ GW. The guiding of 2 TW 1 μm laser pulses can be achieved if the electron density is higher than $n_e > 10^{19}$cm^{-3}. In this regime, the electromagnetic radiation is subject to a host of instabilities. It is natural to expect that instead of the regular plasma wake field that is necessary for the LWFA operation, some irregular Langmuir oscillations will be generated, as was demonstrated in the particle-in-cell simulations by Bulanov *et al.* (1996). The laser pulse guiding and the excitation of the wake field with a regular structure can be provided in a plasma-filled channel created inside a dielectric (such a channel can also be produced in a plasma). As a result, the efficient acceleration of charged particles can be achieved (Bulanov *et al.*, 1996). The experimental demonstration of the laser pulse guiding in a hollow capillary and in a gas-filled capillary were reported by Ehrlich *et al.* (1996) and Hosakai *et al.* (2000), respectively.

Here, we present the results of MHD simulations of plasma discharge inside the capillary channel. Our main objective is to obtain more complete information related to the temporal and spatial evolution of the plasma temperature and density. In Section 2 we formulate the physical model. We present a set of equations of dissipative MHD, formulate the boundary conditions, and describe the plasma–wall interaction. In Section 3 we present the results of computer simulations of the discharge dynamics inside the channel filled initially with argon and inside the initially evacuated channel in the regimes that are typical for the experiments where the X-ray lasing has been achieved. In Section 4 we present results of the capillary plasma dynamics under the parameters optimal for the ultrashort laser pulse guiding. In the final section discussion and conclusions are presented.

2. THE PHYSICAL MODEL

Within the model adopted here the discharge dynamics in different regimes are studied relating to the possible applications of capillary discharges for the X-ray lasers and/or for using capillary plasma to provide a guiding for the ultrashort high-intensity laser pulses. We investigate the discharge dynamics in two types of capillaries: either an evacuated one or one prefilled by preionized or nonionized gas. Since the temperature increases in the course of discharge, a gas ionization occurs, so that the discharge plasma consists of neutral and ionized components. The following phenomena are essential for capillary discharges: the interaction of the plasma with a wall and the ablation of the wall material accompanied by the ionization of the produced gas as well as the interaction of the magnetic field with the plasma (pinch effect). In the parameter range under consideration, it is important to describe the following dissipative processes: electron thermal conductivity, Joule heating, Nernst and Ettinghausen effects, the radiation losses, and ion viscosity. It is also important to incorporate the degree of ionization both into the equation of state and into the dissipation coefficients. We use the approximation of two-temperature (ion and electron) one-

fluid MHD. We assume that the conditions for the local thermodynamic equilibrium are satisfied. These conditions are used to calculate the degree of ionization. Since the length of the capillary is much larger than its diameter, it is reasonable to use the one-dimensional (1D) approximation. Moreover the experiments (Ehrlich *et al.*, 1996; Rocca, 1999) show that the distribution of the discharge parameters along the capillary axis is uniform. The results of 1D simulation also allow us to find the threshold of MHD instabilities, even against the three-dimensional (3D) perturbations with an arbitrary dependence upon all the spatial coordinates (Neudachin & Sasorov, 1993).

2.1. Basic equations

Owing to the large length-to-radius ratio of the capillary ($l/R_0 \gg 1$, where l and R_0 are a length and a radius of the capillary, respectively) a 1D approximation is considered in which all the values depend only on radius r and time t. The relevant MHD equations read:

$$\rho \frac{dv}{dt} = -\frac{\partial p}{\partial r} - \frac{1}{c} jB - \frac{\partial}{\partial r} \Pi_{rr} - \frac{1}{r} (\Pi_{rr} - \Pi_{\varphi\varphi}), \tag{1}$$

$$\frac{d\rho}{dt} = -\rho \frac{1}{r} \frac{\partial}{\partial r} (vr), \tag{2}$$

$$\frac{d}{dt} \frac{B}{\rho r} = \frac{c}{\rho r} \frac{\partial}{\partial r} E_z, \tag{3}$$

$$\rho \frac{d\varepsilon_e}{dt} + \frac{p_e}{r} \frac{\partial}{\partial r} (rv) = jE_z - \frac{1}{r} \frac{\partial}{\partial r} (rq_e) - Q_r + C_{ei}(T_i - T_e), \tag{4}$$

$$\rho \frac{d\varepsilon_i}{dt} + \frac{p_i}{r} \frac{\partial}{\partial r} (rv) = -\frac{1}{r} \frac{\partial}{\partial r} (rq_i) + C_{ei}(T_e - T_i) - \Pi_{rr} \frac{1}{r} \frac{\partial}{\partial r} (rv) - \frac{v}{r} (\Pi_{\varphi\varphi} - \Pi_{rr}). \tag{5}$$

Here $d/dt = \partial/\partial t + v\partial/\partial r$, ρ is the plasma density, $p = p_e + p_i$ is the plasma pressure (it is the sum of the electron and ion pressures), v is the radial component of the plasma velocity, B is the azimuthal component of the magnetic field intensity, Π_{ik} is the ion viscous stress tensor, E_z is the axial component of the electric field in the comoving frame in which the plasma is locally at rest, ε_e and ε_i are the internal specific energies of the electron and ion components of the plasma, related to the unit of the plasma mass, C_{ei} is the rate of thermal transfer between ions and electrons, and T_e and T_i are electron and ion temperatures, respectively. $j = (c/4\pi r)\partial(Br)/\partial r$ is the axial component of the electric current density, q_e and q_i are the radial components of the electron and ion heat fluxes, and Q_r is the rate of radiative energy loss per the unit of volume. We take full account of all dissipative effects in the plasma electron component. In this case we write the generalized Ohm's law in the form as follows

$$E_z = \frac{j}{\sigma_\perp} - \mathcal{N}B \frac{\partial T_e}{\partial r}, \tag{6}$$

$$q_e = -\kappa_\perp \frac{\partial T_e}{\partial r} + \mathcal{N}BT_e j. \tag{7}$$

The second terms on the right-hand side of Eqs. (6) and (7) correspond to the off-diagonal terms in the transport matrix. They describe the so-called Nernst and Ettinghausen effects. The influence of these effects on pinch dynamics was investigated by Bobrova *et al*. (1992). It was shown that the considered effects must be taken into account if the electrons are magnetized. They are of the same order as the electron thermal conductivity and the electric conductivity which are usually taken into account. The expressions for the thermal conductivity $\kappa_\perp$, the Nernst coefficient $\mathcal{N}$, the electric conductivity $\sigma_\perp$, ion viscosity η_0, and the rate of thermal transfer between ions and electrons are taken from the paper by Bobrova and Sasorov (1993), where the well-known system of Braginskii equations (Braginskii, 1963) was generalized for the case of a plasma with a large mean value of the ion charge:

$$\kappa_\perp = \frac{n_e T_e}{m_e \nu_{ei}} \Gamma_1(x_e, w), \tag{8}$$

$$\mathcal{N} = -\frac{1}{m_e c \nu_{ei}} \Gamma_4(x_e, w), \tag{9}$$

$$\sigma_\perp = \frac{e^2 n_e}{m_e \nu_{ei}} (1 - \Gamma_5(x_e, w))^{-1}, \tag{10}$$

$$\eta_0 = 0.96 n_i T_i \nu_{ii}^{-1}, \tag{11}$$

$$C_{ei} = 3 \frac{m_e}{A m_A} n_e \nu_{ei}, \tag{12}$$

where n_e and n_i are the electron and ion densities, e and m_e are the charge and the mass of electron, respectively, A is the atomic number of the element of interest, m_A is the atomic unit of mass. The parameter $x_e = \omega_{Be}/\nu_{ei}$ is large if the electrons are strongly magnetized, and it is small if the influence of the magnetic field upon the dissipative coefficients is negligible. Then, $w = \lambda_{ee}/(\sqrt{2} z \lambda_{ei})$ is the Lorentz parameter for electron gas, characterizing the relative role of electron–electron and electron–ion collisions, and $\Gamma_i(x_e, w)$ are the functions defined in the paper by Bobrova and Sasorov (1993). Thus, the possible considerable difference between λ_{ee} and λ_{ei}, the Coulomb logarithms for electron–electron and electron–ion collisions respectively, is taken into account. The electron–ion and ion–ion collision frequencies are written in the form as follows:

$$\nu_{ei} = \frac{4(2\pi)^{1/2} e^4 z n_e \lambda_{ei}}{3 m_e^{1/2} T_e^{3/2}}, \tag{13}$$

$$\nu_{ii} = \frac{4(\pi)^{1/2} e^4 z^4 n_i \lambda_{ii}}{3 A m_{A^{1/2}} T_i^{3/2}}, \tag{14}$$

where z is the mean ion charge, and λ_{ii} is the Coulomb logarithms for ion–ion collisions. In dense, highly ionized plasmas there is a considerable difference between Coulomb logarithms for electron–electron, electron–ion, and ion–ion collisions. For the parameters typical of capillary discharges, the classical description of the process of Coulomb collisions is accurate enough. We use the following expressions for the Coulomb logarithms:

$$\lambda_{ee} = \frac{1}{2} \ln \frac{9 T_e^3}{16 \pi e^6 n_e}, \tag{15}$$

$$\lambda_{ei} = \frac{1}{2} \ln \frac{9 T_e^3}{4 \pi z^2 e^6 n_e (1 + z T_e / T_i)}, \tag{16}$$

$$\lambda_{ii} = \frac{1}{2} \ln \frac{9 T_i^2 T_e}{16 \pi z^4 e^6 n_e (1 + z T_e / T_i)}. \tag{17}$$

At low temperatures, as long as the mean ion charge is less than unity, there is a noticeable fraction of neutral particles in the plasma. We renormalize the electron–ion collision frequency ν_{ei} by taking into account the contribution of the neutral particles to the electron scattering, whereas the electron–electron collision frequency is assumed to be the same as that in the absence of the neutral atoms. To describe the electron collision with a neutral atom, we adopt the approximation $\sigma_{ea} = \pi a_0^2$ for the transport cross section, a_0 being the Bohr radius. Thus all dissipative coefficients are defined by expressions in which the electron–ion collision frequency is substituted by the effective collision frequency involving the contribution from neutral atoms. These expressions have been applied to both a highly ionized plasma and a plasma with a low degree of ionization. This procedure provides a qualitatively accurate and universal description of limiting cases corresponding to strongly ionized and weakly ionized plasmas, as well as to the transient cases.

The ion component of the plasma is not assumed to be magnetized; hence the viscosity coefficients η_3 and η_4 (Braginskii, 1963) are neglected. In such a formulation, the axial and azimuthal velocity components vanish if they vanish under the initial conditions. For the nonzero components of ion viscosity tensor Π_{ik} we therefore have

$$\Pi_{rr} = \frac{2}{3} \eta_0 \left(\frac{v}{r} - 2 \frac{\partial v}{\partial r} \right), \tag{18}$$

$$\Pi_{\varphi\varphi} = \frac{2}{3} \eta_0 r^2 \frac{\partial}{\partial r} \frac{v}{r^2}. \tag{19}$$

The expression for η_0 has been already introduced.

For the equation of state and the ionization degree, the approximation of local thermodynamic equilibrium is used separately for the electron and ion components. For a mean ion charge $z > 1$, the state of ionization is determined by using the Raizer approximation (Zeldovich & Raizer, 1967) and the mean-ion model. We find the degree of ionization from the condition $\chi(z) + \mu(\rho, T) = 0$, where μ is the chemical potential of an ideal free-electron gas and $\chi(z)$ the ionization potential of a mean ion. For $1 < z < Z/2$, where Z is the atomic number of the element of interest, the average ionization potential is defined by Sommerfeld's formula in the Thomas–Fermi model for the ion shell. For $Z/2 \le z \le Z - 1$, the formula for the hydrogen-like ionization potential is chosen, taking into account the screening of the ion electric field by $(Z - z - 1)$ electrons. For the case $z_0 \le z \le 1$, where $z_0 = 10^{-6}$ is the lowest state of ionization taken into consideration, the simplified Saha formula is used, taking only neutral and once-ionized atoms into account. An ideal gas of free electrons is assumed. The nonideal behavior of the electrons is incorporated only through the ionization potential. In the approximation considered, the free energy of the electron gas is:

$$F_e(V, T_e) = -\frac{z T_e}{A m_A} \left(1 + \ln \frac{1}{2^{1/2} \pi^{3/2}} \frac{V T_e^{3/2}}{z} \right) + \frac{U(z)}{A m_A}, \tag{20}$$

$$U(z) = \begin{cases} \infty & \text{for } z > Z \\ \chi(0) + \int_0^{z-1} \chi(j)\, dj & \text{for } 1 \le z \le Z \\ z\chi(0) & \text{for } 0 \le z \le 1, \end{cases} \tag{21}$$

$$\chi(j) = \begin{cases} \infty & \text{for } j \ge Z - 1 \\ (j+1)^2 / (2(Z - j - 1)^{2/3}) & \text{for } Z/2 - 1 \le j \le Z - 1 \\ (j+1)^{4/3}/2 & \text{for } 0 \le j \le Z/2 - 1, \end{cases} \tag{22}$$

where $F_e(V, T_e)$ is the specific free energy of electron gas, V the specific volume of the atomic cell, and $\chi(j)$ the ionization potential of the mean ion with charge j. All the quantities in Eqs. (20)–(22) are written in atomic units ($e = m_e = \hbar = 1$). The equilibrium state of ionization, $z(V, T_e)$, corresponds to the minimum free energy F_e, treated as a function of three variables, V, T_e, and z:

$$\left(\frac{\partial F_e}{\partial z} \right)_{V, T_e} (V, T_e, z(V, T_e)) = 0. \tag{23}$$

All expressions for the dissipative coefficients of the plasma include the quantity z calculated in such a manner. The specific internal energy ε_e and the pressure p_e are defined as follows:

$$\varepsilon_e(\rho, T_e) = \frac{1}{A m_A} \left[F_e \left(\frac{A m_A}{\rho}, T_e \right) - T_e \left(\frac{\partial F_e}{\partial T_e} \right)_V \left(\frac{A m_A}{\rho}, T_e \right) \right], \tag{24}$$

$$p_e = -\left(\frac{\partial F_e}{\partial V}\right)_{T_e}\left(\frac{Am_A}{\rho}, T_e\right). \quad (25)$$

We assume the ion gas to be ideal also.

For the radiation energy losses, we have used the model description developed by Bobrova *et al.* (1996), which allows us to take into account the line radiation. However, there is no large influence of radiation cooling on plasma dynamics when the magnitude of the electric current is much less than the Pease–Braginskii current value (Braginskii, 1957; Pease, 1957). The Pease–Braginskii current value calculated to take into account line radiation is on the order of several hundreds of kiloamps, whereas in our case, the full electric current does not exceed 30–40 kA.

In our computer simulations, we use the same set of equations to describe both the plasma inside the channel and the adjacent region of the channel wall. This method makes it possible to include a description of the ablation of the wall material, the heating and ionization of this material, and the supply of a heated gas into the plasma discharge region. However, to use this method, we need to specify the equation of state at low temperatures and pressures with allowance for the transition from a solid to a gas state. In our calculations, we used a simple approximation that takes into account the fact that the specific heat of evaporation of the wall material and the specific heat that corresponds to dissociation of molecules into atoms are much less than the specific internal energy of the plasma formed by the gas that was evaporated and ionized. Thus, the capillary wall material is treated as ideal atomic gas and, in the initial conditions of our numerical model, the initial density of the wall material is equal to the real density of this material at fairly low initial temperatures. Our estimates and calculations (Bobrova *et al.*, 1998*a*) show that this approach can be correct for materials that contain hydrogen and have fairly low melting and evaporation points. So the plasma–wall interaction is modeled by considering the material of the wall as a cold neutral gas of high density. Within the model used, the electric conductivity of the wall material can be neglected, as in the case of dielectric wall.

2.2. Initial conditions

Two cases of the discharge plasma dynamics for filled and evacuated capillaries have been simulated. In both cases the discharge is induced by the pulse of the electric current generated by an external electric circuit. In the first case, the capillary channel is prefilled with preionized gas of uniform density and temperature, and in the second case of the evacuated capillaries, the plasma inside the channel is created from the ablation and ionization of the wall material. We must say a few words about the initial conditions under which the current flows in the evacuated capillary. After the threshold voltage is reached, a strongly nonuniform surface breakdown happens at the wall. This stage of the discharge cannot be described by Eqs. (1)–(5) because of the 3D effects and the effects of the plasma quasineutrality disturbance. But this stage is short in time and does not affect the plasma parameters at a later time. For a correct description of the discharge, it is actually sufficient to allow only for the fact that the discharge begins at the wall surface. When the formula for a plasma electric conductivity is used both for high and for low temperatures, the discharge origination near the wall is automatically ensured as the result of the thermal instability at the surface of the wall.

After the breakdown, the impedance of the discharge rapidly becomes small as compared with the total impedance of the power supply circuit. That is why the total electric current through the pinch, $I(t)$, is considered to be a given function of time. The approximation

$$I(t) = I_0\Phi\left(\frac{\pi t}{t_0}\right), \quad (26)$$

where $\Phi(\pi t/t_0)$ is determined by the external electric circuit, is used. Here I_0 is a peak current and t_0 is an effective half-width of the electric current pulse.

3. DISSIPATIVE MHD SIMULATION OF CAPILLARY PLASMAS FOR X-RAY LASERS

A plasma formation in the capillary channels with an electrical discharge is used to generate soft X-ray lasers. The experiments on capillary discharges can be divided into two types. In the first type, the discharge takes place in a channel filled with initially preionized gas. In the second one a surface discharge occurs at the walls of an evacuated channel. It is accompanied by the ablation of the wall material and the creation of the plasma inside the channel.

The dynamics of the discharge plasma in the different regimes is discussed in articles by Bobrova *et al.* (1996, 1998*a*), Lee *et al.* (1996), Rocca *et al.* (1994a), Rocca (1999), and Shlyaptsev *et al.* (1996). Below we present the results of numerical MHD simulations of plasma dynamics inside a capillary with allowance for the plasma–wall interaction both inside evacuated capillaries and in those filled with preionized gas.

3.1. Plasma dynamics in a filled capillary

It is well known that discharge excitation of capillary channels 1.5–5 mm in diameter filled with preionized material has resulted in the compression of a significant fraction of the discharge power into plasma columns of $\sim$300 μm diameter, achieving the high power deposition and the good axial uniformity necessary for soft X-ray lasing. It was shown that a lasing by collisional excitation of Ne-like argon ions takes place when the electron density reaches $0.3\text{–}1 \times 10^{19}$ cm^{-3} and the electron temperature is 60–80 eV (Rocca, 1999). The physical process that has a major impact on the dynamics of the discharge in the prefilled capillary is the ablation of the wall material under the heat flux from the capillary plasma. The ablated material being heated and ionized forms a high

electric conductivity plasma that can lead to significant redistribution of electric current between the initially filling channel argon plasma and the ablated plasma (Bobrova *et al.*, 1996, 1998*a*). Consequently, the discharge dynamics in the filled capillary differ from the classical pinch dynamics (Dyachenko & Imshennik, 1970).

3.1.1. Results of the MHD simulations

In the computer simulations, the capillary channel is initially filled with a preionized gas of uniform density and temperature. A current pulse $I(t)$ is conducted through the plasma, which is assumed to be given by Eq. (26) with $\Phi(\pi t/t_0) = \sin(\pi t/t_0)$ for $0 < t < t_0$.

The overall picture of the discharge can be described as follows: the current pulse heats the plasma and creates the azimuthal component of the magnetic field, thus leading to plasma pinching. A region of nonionized gas of very high density is formed near the wall as the result of the solid matter melting and evaporating. This dense gas is then heated and ionized by the heat flux from the plasma region. Then, it implodes radially towards the capillary axis.

The results of the MHD simulations of a capillary discharge in a 5-mm-diameter channel filled with pure Ar are presented. The initial density of argon is $\rho_0 = 3.2 \times 10^{-7}$ g/cm^3, which corresponds to a pressure of 0.15 Torr at room temperature. The temperature of the argon plasma is assumed to be equal to 0.5 eV. The capillary is made of polyacetal ($(CH_2O)_n$). An equation of state with atomic number $Z = 7$, average atomic weight $A = 14$, and initial density $\rho_0 = 1$ g/cm^3 is used for the wall material. The peak electric current in the circuit is $I_0 = 34$ kA and the half-period of the discharge cycle is 220 ns. The parameters of the discharge are chosen to fit the experiments, the results of which were presented by H.-J. Kunze at the Pisa Easter Conference (April, 1996).

In Figure 1 the capillary discharge evolution is described. Figures 1a and 1b show the lines of constant level of the logarithm of electron density and electron temperature, respectively, and Figure 1c the lines of constant level of the electric current localized inside a region of radius r. The propagation of a compression wave from the capillary wall to the channel axis and its reflection from the neighborhood of the channel axis is apparent. Behind the front of the reflected shock wave, a region of hot and dense plasma (kernel) is formed close to the axis of the channel. It is found that the distribution of the plasma density and temperature are uniform inside the kernel. The kernel lasts for about 10 ns. The maximum plasma parameters achieved in the kernel at $t \approx 64$ ns are $n_e \approx 1.1 \times 10^{19}$ cm^{-3}, and $T_e \approx 51$ eV.

The process of the kernel formation in the capillary discharge may be better understood by looking at the behavior of the current distribution. We note that after $t \approx 40$ ns, a considerable amount of the total current ($\sim$30–40%) is localized near the capillary wall, causing the ablation. It is apparent from Figure 1c that, during the kernel formation, there is practically no current inside the region close to the axis, and less than $\sim$5% of the full current is inside the kernel. For this reason, the formation and the evolution of the kernel, including the converging shock wave, the increase of its amplitude due to the geometry of the capillary, and the resulting increase of the plasma density on the axis, are hy-

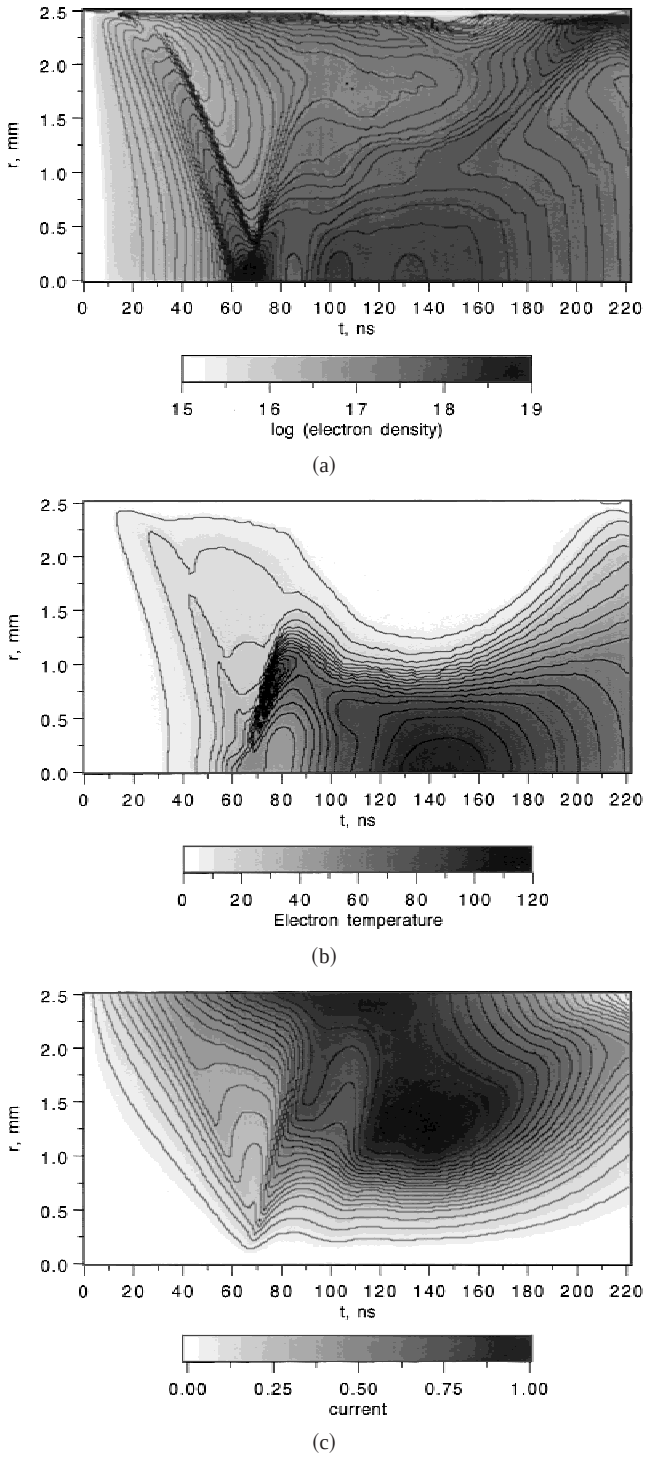

Fig. 1. Results of a computer simulation of capillary discharge dynamics in a 5-mm-diameter channel filled with 0.15 Torr of pure Ar at a current $I_0 =$ 34 kA, and half-cycle time $t_0 = 220$ ns. (a) Lines of constant value of decimal logarithm of electron density measured in cm^{-3}. (b) Lines of constant value of the electron temperature measured in eV. (c) Lines of constant value of electric current inside the region with radius r, normalized over I_0.

drodynamic processes, contrary to what is seen in classical *Z*-pinches, where the magnetic forces play the main role in the plasma acceleration till the moment of its maximum compression, as had been shown by Dyachenko and Imshennik (1970). It must be noted that the formation of the converging shock wave is due to the action of the Ampere force $[\vec{j} \times \vec{B}]$ in the initial stage of the discharge. Nevertheless, after the time $t \sim 50$ ns the influence of the magnetic field on the argon–plasma dynamics can be ignored. There are two stages of energy conversion. In the first stage the energy of the magnetic field is transferred to the argon plasma in the form of kinetic energy. Then during the reflection of the converging shock wave from the central region, the kinetic energy is converted into the thermal energy of the compressed and heated plasma kernel. The ablation flow slowing down leads to an additional plasma compression for $t > 80$ ns.

As long as the magnetic pressure does not play a significant role in the kernel formation, some additional investigation seems to be desirable to explain the high plasma compression extent in the kernel (more than 200-fold). This resulting compression appears to be 10 times greater as compared to the *limiting* compression of the fully ionized plasma in a cylindrical imploding shock wave. We explain the enhanced compression by the plasma thermal energy losses due to the ionization (see Bulanov & Sokolov, 1997).

The radial distributions of the electron density at different time moments are shown in Figure 2. At $t = 57$ ns, we see the converging shock wave that creates a concave density profile, observed by Hosokai *et al.* (2000). Upon the shock wave reaching the axis, the local minimum of the electron density on the axis disappears, and at $t = 65$ ns, we see that the kernel is formed. At $t = 100$ ns, the electron density distribution becomes smooth, slightly decreasing from the axis to the periphery of the discharge. The radial distributions of plasma parameters inside the channel at $t = 64$ ns are plotted in Figure 3. Figure 3a shows the profiles of the electron density, the electron, and ion temperatures, and Figure 3b shows the radial distributions of electric current density and plasma velocity. One can see a significant increase in the electron density, temperatures, and electric current density near the axis of the channel. Near the walls, the plasma parameters are also strongly nonuniform. The electron and ion temperatures are close to each other elsewhere, except the front of the diverging shock wave. The radial dependence of the current density confirms the above conclusion that the electric current separates into two spatially independent components flowing in the argon plasma and in the peripheral regions of the discharge. A contact discontinuity separating the argon plasma that initially fills the channel from the plasma that is produced via ablation of the capillary wall material is seen near $r \approx 0.5$ mm. In Figure 3b the radial distribution of the plasma velocity is shown. Near the wall, an expansion of the plasma towards the axis without any shock wave is observed. The plasma flow slows down near $r \approx 0.75$ mm due to interaction with the magnetic field of the discharge. Near the kernel boundary, a sharp discontinuity in the plasma velocity is observed, which is associated with the front of the shock-wave. Between the shock-wave front and the region where the plasma flow quickly slows down,

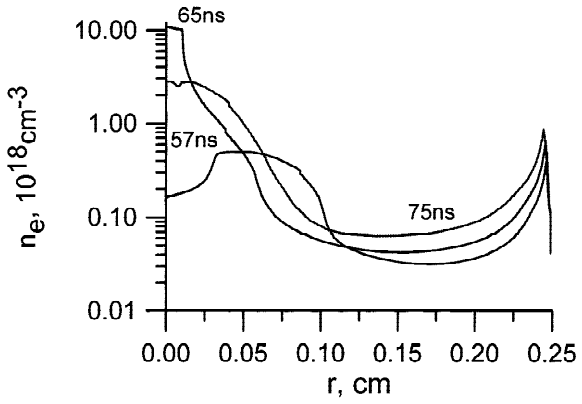

Fig. 2. Radial distribution of electron density n_e at three different moments of time, for the same parameters as in Figure 1.

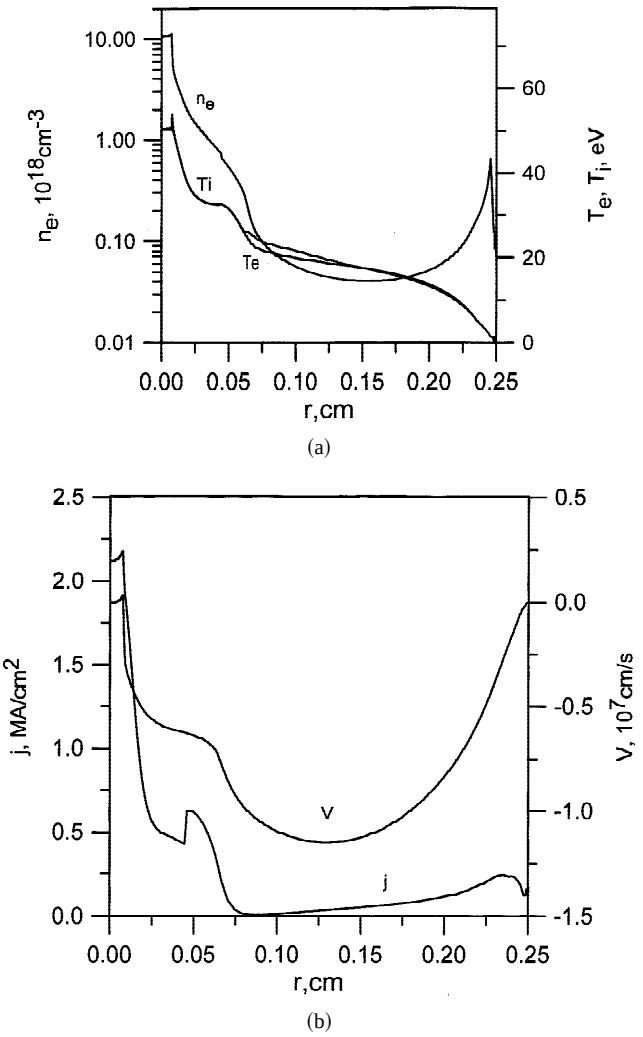

Fig. 3. Radial distribution of (a) electron density n_e, and electron and ion temperatures T_e, T_i, and (b) electric current density j and plasma velocity v at $t = 64$ ns, for the same parameters as in Figure 1.

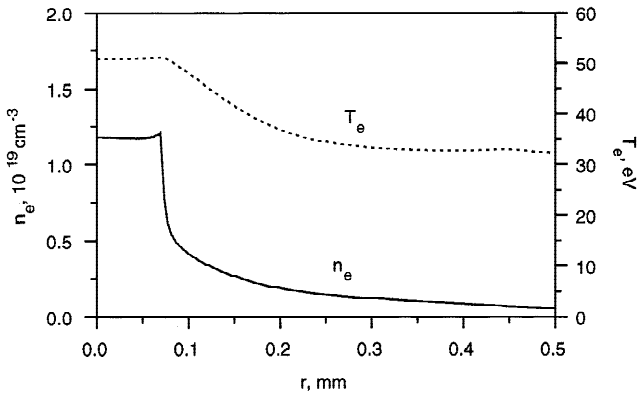

Fig. 4. Radial distribution of electron density n_e and electron temperature T_e inside the kernel at moment $t = 64$ ns, for the same parameters as in Figure 1.

the velocity remains constant. The region $r < 0.1$ mm is occupied by high-density hot plasma. The radial distributions of electron temperature and density inside the kernel are plotted in Figure 4. This relatively short-lived dense, hot kernel on the channel axis is likely to be the site of the laser wave amplification. We expect that an account of two-dimensional effects should not modify our conclusion about the formation of the dense, hot kernel with uniform plasma density and temperature in the axis of the channel. The instabilities may not be very important, because the degree of compression in the considered case is moderate. Moreover, the experiments (Rocca, 1999) show high homogeneity of the kernel plasma along the axis.

Our simulation (Bobrova *et al.*, 1998*a*) of the capillary discharge with the parameters chosen to fit the experimental conditions of Rocca *et al.* (1994*a*) shows good agreement with experimental results. Experimental and calculated kernel size and lifetime were in close agreement, and the observed time of plasma compression has coincided with the simulation time.

All the simulations of the discharge dynamics were performed for plastic capillaries because the adopted model of plasma–wall interaction is valid for this material. In the case of a ceramic or a quartz capillary, it would be better to take into account the specific heat of evaporation of the wall material and the specific heat that corresponds to dissociation of molecules into atoms. We investigated the influence of the ablation of the wall material on the discharge dynamics. We have simulated the fast *Z*-pinch dynamics in a quartz tube (Wagner *et al.*, 1996). In the first run, we did not take the ablation of the wall material into account, whereas in the second run, the ablation was taken into account according to the model of the plasma–wall interaction adopted in the present article. Upon comparing the simulation results for the two runs with the experimental data, it is possible to show that the ablation is significant even for quartz tubes of a diameter of 1–2 cm. The results obtained in the first run differed greatly from experimental ones, whereas the second-run results were much closer to those obtained in the experiment. Thus, we can conclude that the adopted model of plasma–wall interaction can be used for simulation of capillary discharges.

3.1.2. Dimensionless parameters

The investigation of plasma dynamics in discharges from capillaries filled with preionized gas involves many parameters, such as the initial radius of the channel R_0, the initial density of the plasma ρ_0, the electric current amplitude I_0, and the current half-period t_0. Here, we address the regimes in which the initial temperature of the plasma, and hence the sound velocity, are low enough so that the perturbation imposed from the boundary propagates inside the channel as a strong shock wave. To simplify the investigation of the problem, it is of great importance to find dimensionless parameters describing the relative role of different processes.

The velocity of the shock wave inside the channel can be estimated to be on the order of the Alfvén velocity, $v_A = B/(4\pi\rho_0)^{1/2}$, with the magnetic field $B = 2I_0/cR_0$. Assuming a typical time scale, $t_c = R_0/v_A$, we obtain

$$t_c = (\pi\rho_0)^{1/2}\,\frac{cR_0^2}{I_0}. \tag{27}$$

The ratio between t_c and the half-period of the electric current t_0 is the first dimensionless parameter

$$\frac{t_c}{t_0} = \frac{(\pi\rho_0)^{1/2}cR_0^2}{I_0 t_0}. \tag{28}$$

There are also the other dimensionless parameters describing the role of dissipative processes near the axis, related to the electron thermal conductivity and the plasma resistivity,

$$\frac{R_0}{r_\chi} = \left(\frac{I_0}{(\pi\rho_0)^{1/2}c\chi}\right)^{1/2} \tag{29}$$

and

$$\frac{R_0}{r_\sigma} = \left(\frac{I_0}{(\pi\rho_0)^{1/2}c\nu_m}\right)^{1/2}, \tag{30}$$

where the typical scale of the temperature nonuniformity is $r_\chi \approx \chi/v_A$, and the scale of the magnetic field nonuniformity is $r_\sigma \approx \nu_m/v_A$, $\chi = \kappa_\perp/c_V$, $\nu_m = c^2/4\pi\sigma$, and c_V is the specific heat of the electron component.

On the scales of channel radius, dissipative effects are negligible in the regimes considered in this subsection. Nevertheless, close to the walls, near the channel axis, and at the shock-wave fronts, dissipative effects determine the typical scales of nonuniformity. It can be shown that the typical scale of the temperature nonuniformity near the wall is $r_\chi = \chi cR_0(\pi\rho_0)^{1/2}/I_0$, and the scale of the magnetic field nonuniformity near the wall is $r_\sigma = \nu_m cR_0(\pi\rho_0)^{1/2}/I_0$.

We first briefly analyze the role of the parameter t_c/t_0. In the physical situation under examination, it actually governs the dynamics of the shock wave, and determines the time at

which the kernel is formed. Note that if the value of t_c/t_0 is increased over a critical value, the formation of the kernel is not observed in the time interval t_0. At constant t_c/t_0, the $r-t$ plots are found to be self-similar: the dynamics of the shock wave are almost the same.

We characterize the performances of the discharge in terms of the physical quantities in the kernel, in particular its maximum density and temperature, and determine their dependence on the parameters of the discharge. To do this, we fix the value of $t_c/t_0 \sim 0.35$, corresponding to the experiment performed by Rocca *et al.* (1994*a*), and investigate the behavior of the maximum density and temperature $\rho_{\max}$, and $T_{e\,\max}$, while the other parameters are varied. From the performed series of computations, the following scalings are obtained (Bobrova *et al.*, 1998*a*)

$$T_{e\,\max} \approx 60\,\frac{R_0'}{t_0'}\ \text{eV}, \tag{31}$$

$$\rho_{\max} \approx 270\left(\frac{R_0'}{t_0'}\right)^{-0.3-2.5\lg(R_0'/t_0')} \rho_0'^{3/4} I_0'\,\frac{\mu\text{g}}{\text{cm}^3}, \tag{32}$$

where the primed variables are normalized in the following way: $R_0' = R_0$ (mm)/2, $t_0' = t_0$ (ns)/60, $I_0' = I_0$ (kA)/40, and $\rho_0' = \rho_0\ (\mu\text{g/cm}^3)/1.37$.

3.2. Capillary discharge in an evacuated channel

In the evacuated capillaries, a surface discharge occurs at the walls of the channel. It is followed by the ablation of the wall material and the creation of a plasma inside the channel. The possibility of obtaining a laser wave amplification by collisional recombination in capillary discharge plasmas was proposed by Rocca *et al.* (1988), who analyzed the case of amplification at 18.2 nm in the 3–2 line of H-like C. Evidence of lasing has been reported in several discharge-pumped recombination laser experiments (Steden & Kunze, 1990; Shin *et al.*, 1994; Dussart *et al.*, 1999). However, in all cases only a small increase in the line intensity has been observed.

3.2.1. Results of the MHD simulations

The results of MHD simulations of discharge dynamics in an initially evacuated channel are discussed. The plasma inside the channel is produced from the polyethylene walls.

In Figure 5 the evolution of the capillary discharge is described. The parameters of the discharge are chosen to fit the experiment performed by Shin *et al.* (1994). The radius of the channel is $R_0 = 0.6$ mm. The electric current in the external circuit is determined by Eq. (26) with $\Phi(\pi t/t_0) = \sin(\pi t/t_0)$ for $0 < t < t_0$, $I_0 = 25$ kA, and the half-period $t_0 = 220$ ns. Figures 5a and 5b show the lines of constant value of the logarithm of plasma density and the plasma temperature, respectively, and Figure 5c displays the lines of constant value of the electric current localized inside a region of radius r. At the initial stage, a fast plasma compression occurs from a channel's periphery to its axis. Subsequently the plasma density changes smoothly in time. The transient process is easily seen in Figure 5. In the outer region of the discharge, plasma contraction changes to plasma expansion that is governed by both the reflection of the shock wave and

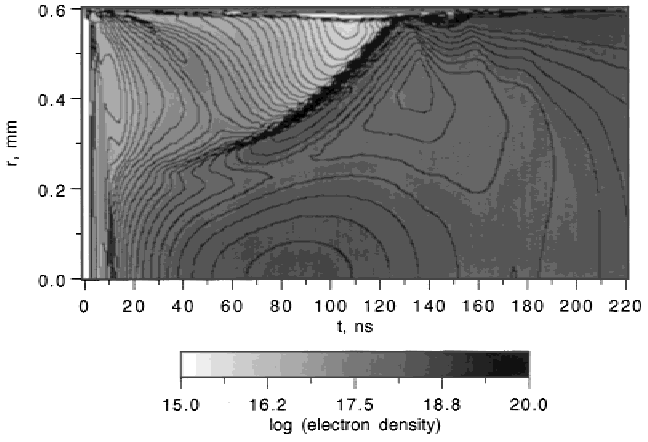

(a)

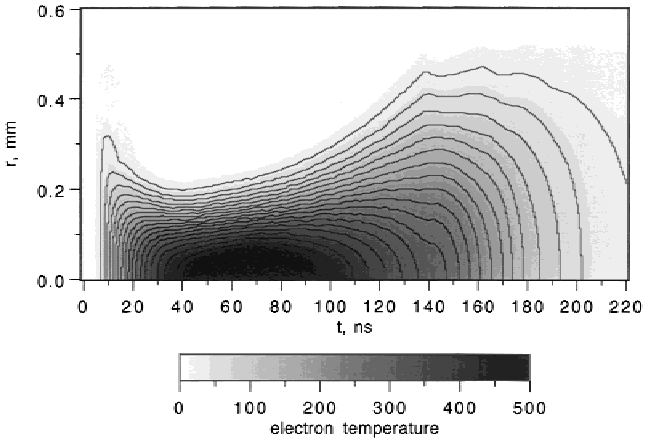

(b)

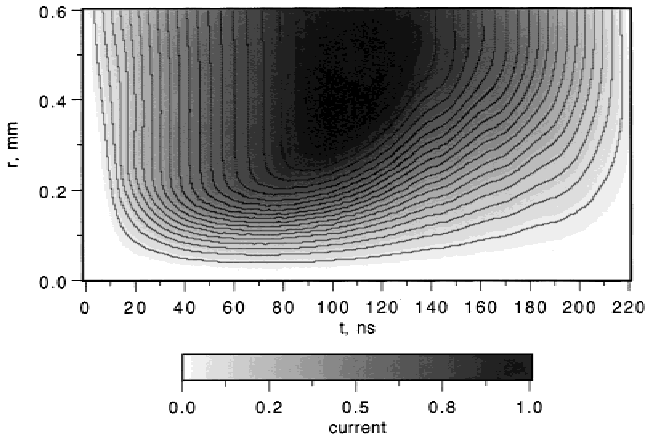

(c)

Fig. 5. Results of computer simulation of capillary discharge dynamics in a 1.2-mm-diameter evacuated channel at a current $I_0 = 25$ kA, and half-cycle time $t_0 = 220$ ns. (a) Lines of constant value of decimal logarithm of electron density measured in cm^{-3}. (b) Lines of constant value of the electron temperature measured in eV. (c) Lines of constant value of electric current inside the region with radius r, normalized over I_0.

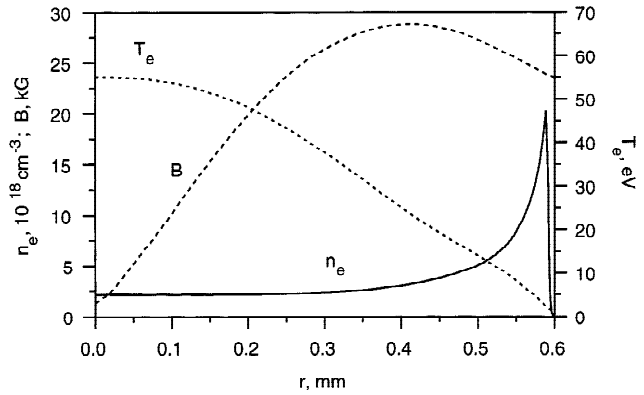

Fig. 6. Radial distribution of electron density n_e and electron temperature T_e at moment $t = 200$ ns, for the same parameters as in Figure 5.

plasma heating in the region close to the axis. Then the radial distribution of plasma density and temperature inside the channel becomes smoother. The variation characteristic scale is on the order of the capillary diameter. The pinch occupies almost the whole channel.

The electric current flows in the vicinity of the channel axis during the first stage of the discharge, then the radial distribution of the electron current density becomes smooth, as shown in Figure 5c.

In Figure 6 the radial distributions of the plasma parameters at $t = 200$ ns are given. This time is chosen to show the typical plasma parameters distribution in the quasiequilibrium stage, when there is both mechanical equilibrium (the Ampere force is balanced by the plasma pressure gradient) and thermal quasiequilibrium (Joule heating is balanced by the heat outflow due to thermal conductivity and radiative energy losses). The radial distributions of the plasma parameters are in good agreement with the experimental data. The difference between the calculated values of the plasma density and temperature and those obtained in the experiment is not substantial. Our model gives somewhat overestimated plasma temperature and underestimated density of the discharge plasma. According to the estimates, the plasma in the central region of the discharge is at a mechanical equilibrium for a time that markedly exceeds the characteristic Alfvén time, and the dissipative processes are not so important on this time scale. In these conditions the different ideal and dissipative MHD instabilities can be expected to occur inside the channel (Bobrova *et al*., 1996). These instabilities can lead to the excitation of MHD turbulence, and a change in the transport processes. In Bobrova *et al*. (1996) we investigated the possible influence of an anomalous transport on the parameters of the capillary discharge under the conditions corresponding to the experiment by Steden and Kunze (1990). Our simulations showed that by incorporating the additional turbulent transport as well as the correspondent Joule heating, we decrease the plasma temperature and increase the density. Comparing the results of calculations with experimental data we can conclude that MHD turbulence plays an important role in discharge dynamics in evacuated capillaries for X-ray lasers.

We pay attention to the contradiction between the maximum electron temperature obtained in simulations and measured in experiments, on one hand, and the temperature required for explaining the presence of a noticeable fraction of highly ionized C^{5+} carbon ions, observed in the experiments, on the other hand. The possible mechanisms of generation of C^{5+} ions were discussed by Kunze *et al*. (1994), Bobrova *et al*. (1996), and Bulanov *et al.* (1997b). We assume that the existence of C^{5+} ions can be explained by the properties of the plasma implosion in the evacuated channel.

3.2.2. Formation of the hot plasma region near the channel axis

We can see that the temperature of the plasma after convergence of the plasma flow towards the channel axis is significantly higher in the initially evacuated channel than in the case of the channel initially prefilled by a plasma. This can be explained if one takes into account a specific property of the convergent plasma flow to create a high-entropy region. Such a phenomenon in the case of 1D plane geometry has been predicted by Stanyukovich (1960). The case of cylindric symmetry has been studied recently by Askar'yan *et al.* (1999).

The formation of the high-entropy region with an extremely high temperature at the channel axis after the plasma flow converges is neither due to acceleration of the flow (the flow velocity, v, is finite) nor due to plasma heating at the shock-wave front (the temperature growth is proportional to v^2), but with the specific behavior of the entropy at the shock front: the entropy can tend to infinity even for a finite difference between the value of the temperatures ahead and behind the shock front, if the plasma density ahead of the shock front vanishes.

To demonstrate this property we assume that the plasma density inside the channel changes from ρ_0 near the channel wall down to $\rho_1 \ll \rho_0$ at the axis. Converging toward the axis, the plasma flow is slowing down at the shock front. At the shock front the plasma density increases in a factor $(\gamma + 1)/(\gamma - 1) \approx 4$; meanwhile the plasma temperature behind the shock front is proportional to v^2, being on the order of T_0. The characteristic for the entropy value $T/\rho^{\gamma-1}$ increases up to $T_0/\rho_1^{\gamma-1}$. It tends to infinity when $\rho_1/\rho_0 \to 0$. Later on when the plasma pressure at the axis grows adiabatically up to the value $\approx P_0$, the temperature increases up to $T_0(\rho_0/\rho_1)^{(\gamma-1)/\gamma} \gg T_0$; meanwhile the density becomes on the order of $\rho_0^{1/\gamma}\rho_1^{(\gamma-1)/\gamma}$.

4. DISSIPATIVE MHD SIMULATION OF CAPILLARY PLASMAS FOR GUIDING OF INTENSE ULTRASHORT LASER PULSES

As we noted in the Introduction the channel produced in a solid insulator and prefilled by plasma (the channel can also be produced in the plasma) provides optimal conditions for both the guiding of the laser pulse and for the excitation of

the wake field with a regular structure. The dynamics of a capillary discharge to achieve the optimum conditions for the guiding of laser pulses have been studied by Bobrova *et al.* (1998*b*, 2000). The experimental demonstration of the laser pulse guiding in a plasma waveguide formed near the axis of the capillary discharge was reported by Ehrlich *et al.* (1996) and Hosakai *et al.* (2000).

4.1. Parameters of the capillary required for laser pulse guiding

Let us write the expressions for the acceleration length, l_{acc}, and effective radius of the region in which electromagnetic radiation is localized, r_w, in a plasma channel with the parabolic profile of the electron density $n_e(r) = n_e(0) + n_e''(0)r^2/2$:

$$l_{acc} = \frac{\lambda}{2\pi}\left(\frac{n_{cr}}{n_e(0)}\right)^{3/2}, \tag{33}$$

$$r_w = (\lambda R_0)^{1/2}\left(\frac{n_{cr}}{2\pi^2 n_e(0)}\right)^{1/4}\left(\frac{n_e(0)}{n_e''(0)R_0^2}\right)^{1/4}. \tag{34}$$

Here the radius of the channel, R_0, is supposed to be larger than r_w, and the critical density, defined by the condition $\omega_{pe} = \omega_0$, n_{cr}, is larger than $n_e(0)$. Here ω_0 is the carrier frequency. We see that the transverse size of the electromagnetic mode localization, r_w, in the parabolic density channel is on the order of $(n_e(0)d_e^2/n_e''(0))^{1/4}$, where $d_e = c/\omega_{pe}$.

In the case of the glass laser with the wavelength of the radiation equal to 1 μm, we need to use the waveguide with $r_w \approx 10$ μm. The channel is supposed to be filled with a plasma of the density on the order of $\approx 10^{19}$ cm^{-3} at the axis. In the case of the CO_2 laser with the wavelength of the radiation equal to 10 μm, one needs to use the waveguide with $r_w \approx 100$ μm, filled by a plasma with the density on the order of $\approx 10^{17}$ cm^{-3} [see the discussion in an article by Pogorelsky *et al.* (1996)].

The plasma configurations with such parameters can be produced in the capillary discharges. Our MHD simulations of the capillary plasma dynamics (Bobrova *et al.*, 1996) revealed the regimes in which the plasma parameters are close to those required for the laser pulse guiding.

Since the plasma dynamics in the capillaries show very complicated dependence on the wall material, the composition of the plasma inside the channel, and on the external electric circuit (Bobrova *et al.*, 1996, 1998*a*, 1998*b*), extensive studies of the capillaries for the laser pulse guiding are needed. With MHD simulations we want to demonstrate the range of the parameters in which the suitable conditions for the laser pulse guiding and the wake-field excitation can be reached.

We can see in Figure 6 the formation of a smooth plasma density profile with the local minimum of the electron density on the channel axis. This radial profile is typical for the late stages of capillary discharge dynamics. An efficient guiding of the laser pulses can be expected in channels with such radial profiles if necessary values of electron density on the axis and the transverse size of the electromagnetic mode localization, r_w, can be achieved.

4.2. Capillary discharge free of instabilities

Because the fluctuations of electron density caused by the MHD turbulence can destroy a regular structure of the plasma wave, they may prevent a proper acceleration process. For this reason it is necessary to find discharge regimes that will be free of MHD instabilities. It is well known that *Z*-pinch with strong electric current in the absence of walls is unstable against various MHD modes. At the same time, a sufficiently symmetric first compression is achievable in many experiments. We expect that capillary discharge is free of MHD instabilities for the regimes when the electric current inside the plasma has already decayed after the first plasma compression. In this case, the plasma density distribution with parabolic profile can remain unchanged.

To achieve such a regime of capillary discharge dynamics, it is necessary to switch off the electric current at a certain moment of time. It is well known that *Z*-pinch is stable during the first compression and subsequent expansion till the moment at which the pinch radius becomes maximum. Consequently, if we switch off the current during the plasma expansion after the shock wave has converged on the axis, then MHD instabilities will not develop. Even if MHD instabilities have developed during the current pulse, they are damped after the pulse is switched off. To receive an aperiodic current pulse, the external electric circuit formed by the capacity of the source, C, and the inductance of the circuit itself, L, should be supplemented by the Ohmic resistance

$$\mathcal{R} = 2(L/C)^{1/2}. \tag{35}$$

Then the current pulse is shaped as:

$$I(t) \propto te^{-t/t_0}, \tag{36}$$

where $t_0 = (LC)^{1/2} = t_{1/2}/(\pi/3)$, and $t_{1/2}$ is a half-period of current pulse in the absence of Ohmic resistance.

To describe the capillary discharge dynamics, we use the dimensionless parameter $t_c/t_0 = (\pi\rho_0)^{1/2}cR_0^2/(I_0 t_0)$, which is the ratio between the typical plasma time scale t_c and the external circuit time scale t_0. Here t_c is the time for a shock wave to reach the channel axis. We have already noted that at a constant value of the parameter t_c/t_0, the trajectories of plasma elements in the *r-t* plane are found to be self-similar. As it follows from MHD simulations by Bobrova *et al.* (1998*a*) the dynamics of the shock wave are almost the same for different capillary discharges with constant value of t_c/t_0. This indicates that, under the condition $t_c/t_0 \sim 1$, the plasma in experimental devices with parameters similar to those considered below should be free of MHD instabilities. We also choose the pulse to be short enough so that MHD instabilities have no time to develop. Then, after switching off the current, the plasma remains stable. Below we shall

keep the parameter t_c/t_0 constant. Subsequent slow cooling of the current-free capillary plasma surrounded by the ablating cold capillary wall causes typical spatial distribution of plasma density and temperature with almost constant pressure.

4.3. Results of MHD simulations

To optimize the values of electron density on the axis and the radius of the electromagnetic mode localization r_w, we performed simulations of the discharge dynamics in the capillary filled with the nitrogen. The dimensionless parameter t_c/t_0 was on the order of 1.

For a CO_2 laser with a wavelength of 10 μm, we choose the following initial conditions. The radius of the channel is $R_0 = 2.5$ mm. The electric current in the external electric circuit is determined by Eq. (36) with peak electric current $I_0 = 32$ kA and $t_0 = 20$ ns. The channel is filled with pure nitrogen at an initial density $\rho_0 = 3.0 \times 10^{-7}$ g/cm^3. The capillary walls are of polyacetal ($(CH_2O)_n$). At $t = 200$ ns, when electric current had already vanished and plasma is in quasiequilibrium, electron density on the axis equals $n_e = 2.5 \times 10^{17}$ cm^{-3}, the radius of the electromagnetic mode localization equals $r_w = 140$ μm, and electron temperature is $T_e = 28$ eV. These parameters, slightly changing, exist for approximately 50 ns. Spatial distributions of the electron density and temperature are shown in Figure 7. The plasma dynamics in such capillaries will be discussed below for the capillary filled with deuterium.

For a 1-μm laser we considered the capillary discharge with peak electric current $I_0 = 30$ kA and $t_0 = 6.6$ ns, in a 0.6-mm-diameter channel filled with nitrogen at an initial density $\rho_0 = 5.2 \times 10^{-5}$ g/cm^3. At $t = 60$ ns the electron density radial distribution has a parabolic profile, the electron density on the axis equals $n_e = 1.5 \times 10^{19}$ cm^{-3}, the radius of the electromagnetic mode localization equals $r_w = 20$ μm, and the electron temperature is $T_e = 15$ eV. It is necessary to pay attention to the fact that r_w depends on $n_e'' R_0^2/n_e$, which is a function of time. In the cases under consideration it is on the order of 1 and it is possible to find a time interval of $\approx$50 ns during which the $n_e'' R_0^2/n_e$ change is not significant.

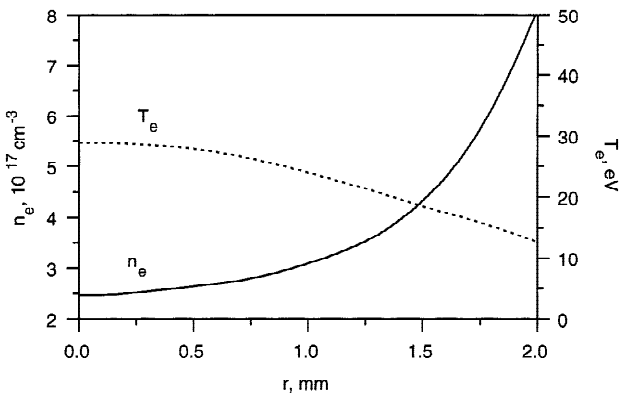

Fig. 7. Radial distribution of electron density n_e and electron temperature T_e at moment $t = 200$ ns in a 5-mm-diameter channel filled with nitrogen with initial density $\rho_0 = 3.0 \times 10^{-7}$ g/cm^3 at a current $I_0 = 32$ kA, and $t_0 = 20$ ns.

However the capillaries filled with nitrogen do not provide optimal conditions because of the laser pulse depletion due to the ionization of the gas. To diminish the ionization losses it is better to fill the capillaries with hydrogen or deuterium, although, in such channels, the condition $t_c/t_0 \sim 1$ is far more difficult to satisfy.

The results of MHD simulation of a capillary discharge in a channel filled with pure deuterium are presented. The version for a CO_2 laser corresponds to a capillary with radius $R_0 = 2.8$ mm, initial plasma density $\rho_0 = 3.5 \times 10^{-7}$ g/cm^3, and electron temperature of 1.0 eV. The capillary is of polyacetal ($(CH_2O)_n$). An equation of state with atomic number $Z = 7$, average atomic weight $A = 14$, and initial density $\rho_0 = 1$ g/cm^3 is used for the wall material. The peak current in the circuit is $I_0 = 30$ kA and the external circuit characteristic time is $t_0 = 23$ ns.

In Figure 8 the evolution of the capillary discharge is described. Figures 8a and 8b show the lines of constant value of the logarithm of electron density and the electron temperature, respectively, and Figure 8c the lines of constant value of the electric current localized inside a region of radius r. Plasma dynamics are very similar to those of filled capillaries already discussed (compare Fig. 1 and Fig. 8). We can see the propagation of a compression shock wave from the wall toward the axis of the channel, the reflection of this wave from the region near the axis, and its turn into a diverging shock wave. The contact discontinuity, where the plasma arising during the ablation of the wall material comes into contact with the deuterium plasma that filled the channel initially, is easily seen in Figure 8a. The fall of the electron density near the channel wall is caused by the decreasing of plasma temperature and state of ionization while plasma density is increasing. Figure 8c displays lines of constant value of the electric current inside the region with radius r, normalized over the peak current in the circuit I_0. After $t = 100$ ns, the electric current vanishes and plasma inside the capillary is in quasiequilibrium. The time evolution of the electron density and temperature on the axis are plotted in Figure 9, showing that after $t = 150$ ns, electron density on the axis is constant for $\sim$100 ns. The electron temperature on the axis slowly decreases with time. Note that, for the electron density and temperature to evolve so smoothly, the governing characteristics of the current pulse, channel radius, and initial gas density should be adjusted accordingly. Otherwise we should observe relaxation oscillations, in the course of which the plasma density and temperature change on the time scale required for the shock wave to propagate over the distance on the order of the channel radius. The radial distributions of electron density and temperature at $t = 250$ ns are plotted in Figure 10. Electron temperature slowly decreases to the walls of the capillary. In the vicinity of the axis it is uniform. The contact discontinuity between

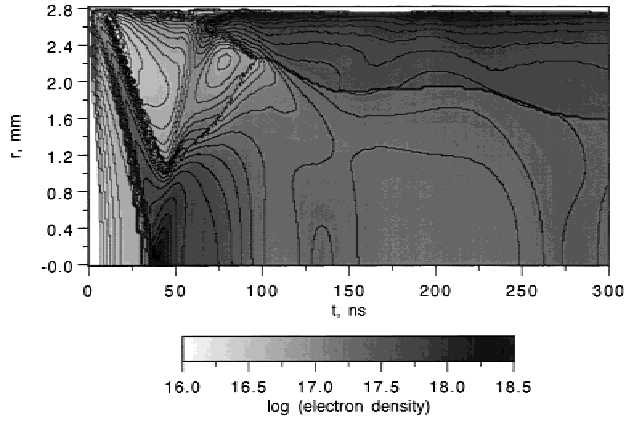

(a)

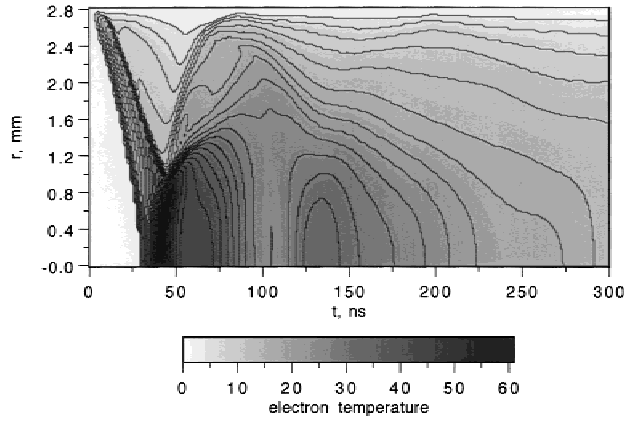

(b)

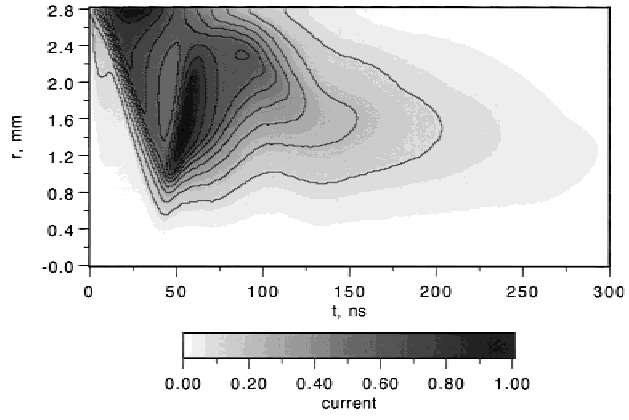

(c)

Fig. 8. Results of a computer simulation of capillary discharge dynamics in a 5.6-mm-diameter channel filled with deuterium with initial density $\rho_0 = 3.5 \times 10^{-7}$ g/cm^3 at a current $I_0 = 30$ kA, and external circuit characteristic time $t_0 = 23$ ns. (a) Lines of constant value of decimal logarithm of electron density measured in cm^{-3}. (b) Lines of constant value of the electron temperature measured in eV. (c) Lines of constant value of electric current inside the region with radius r, normalized over I_0.

the deuterium plasma and the ablated plasma is seen at $r =$ 1.8 mm. The electron density in deuterium plasma has a parabolic profile with the minimum $n_e = 2 \times 10^{17}$cm^{-3} on the axis. The radius of the electromagnetic mode localization equals $r_w = 170$ μm, and the electron temperature is $T_e = 18$ eV.

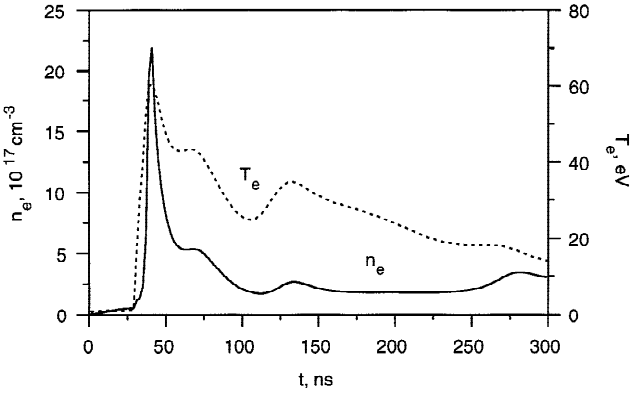

Fig. 9. Temporal evolution of electron density n_e and electron temperature T_e on the axis, for the same parameters as in Figure 8.

The version for a 1-μm laser corresponds to a capillary with radius $R_0 = 0.23$ mm, initial density of deuterium $\rho_0 = 4.5 \times 10^{-5}$ g/cm^3, and electron temperature of 1.0 eV. The electric current in the external electric circuit is determined by Eq. (36), with peak electric current $I_0 = 10$ kA and $t_0 = 10$ ns.

In Figure 11 the evolution of the capillary discharge is described. In the case under consideration, the process of the converging and reflecting of the compression shock wave takes a relatively short time, then the plasma column oscillates, but the oscillations decay with time. After $t = 100$ ns, plasma is in quasiequilibrium with slightly decreasing electron density and temperature. Figure 11c shows that, for these moments of time, plasma is free of electric current. The contact discontinuity between the deuterium plasma and the plasma arising during the ablation of the wall materials is near the walls and does not move to the axis. It means that after the transition period, the ablation stopped. The time evolution of the electron density and temperature on the axes are plotted in Figure 12. The radial distribution of electron

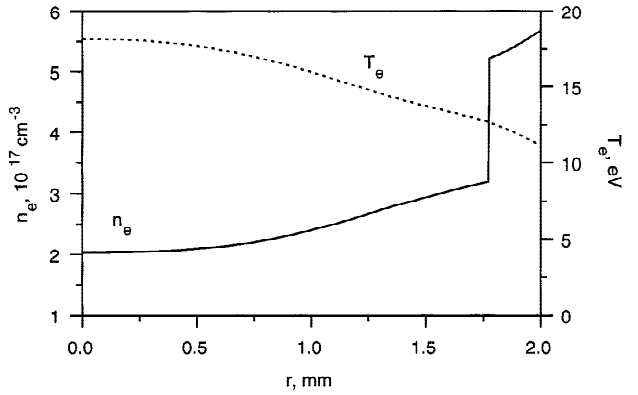

Fig. 10. Radial distribution of electron density n_e and electron temperature T_e at moment $t = 250$ ns, for the same parameters as in Figure 8.

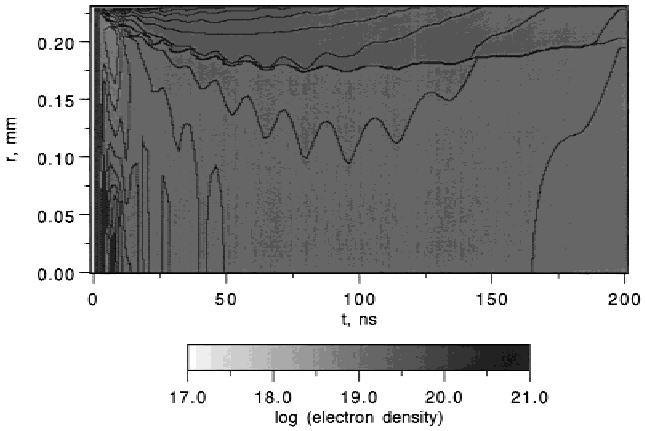

(a)

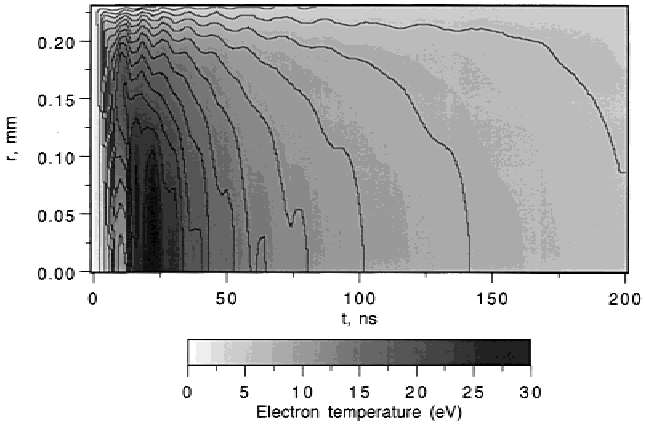

(b)

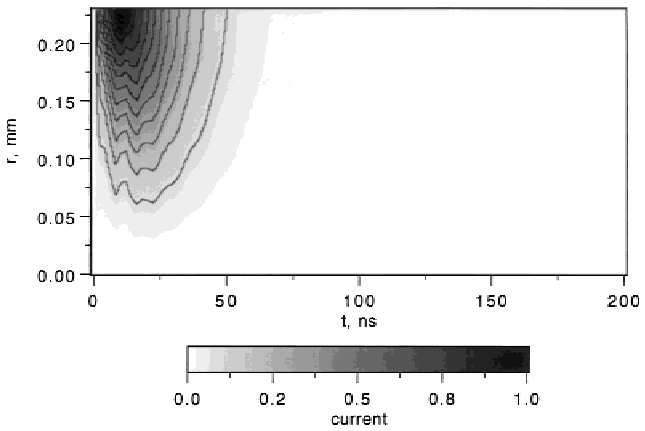

(c)

Fig. 11. Results of a computer simulation of capillary discharge dynamics in a 0.46-mm-diameter channel filled with deuterium with initial density $\rho_0 = 4.5 \times 10^{-5}$ g/cm^3 at current $I_0 = 10$ kA and external circuit characteristic time $t_0 = 10$ ns. (a) Lines of constant value of decimal logarithm of electron density measured in cm^{-3}. (b) Lines of constant value of the electron temperature measured in eV. (c) Lines of constant value of electric current inside the region with radius r, normalized over I_0.

density and the temperature near the axis at $t = 100$ ns are plotted in Figure 13.The electron density in deuterium plasma has a parabolic profile with the minimum $n_e = 2.0 \times 10^{19}$ cm^{-3} on the axis. The radius of the electromagnetic mode

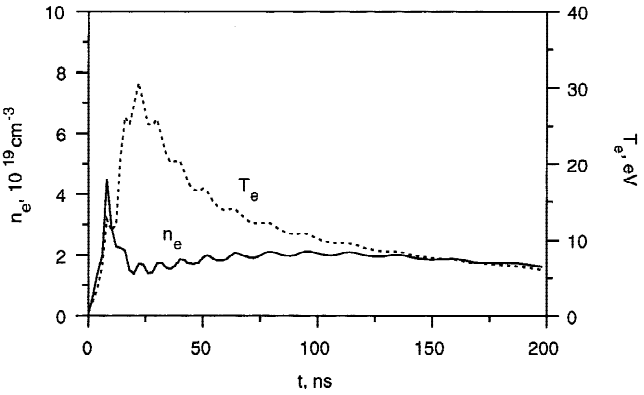

Fig. 12. Temporal evolution of electron density n_e and electron temperature T_e on the axis, for the same parameters as in Figure 11.

localization equals $r_w = 20$ μm, and the electron temperature is $T_e = 10$ eV.

5. DISCUSSION AND CONCLUSIONS

We have investigated different regimes of the capillary discharge dynamics. In regards to the capillary discharges for the X-ray lasers, we have analyzed the two regimes of the capillary discharge dynamics inside the channel. In the first case, the channel is filled with preionized gas; in the second one, the material in the plasma comes from ablation of the wall.

In the first regime, the hydrodynamical effects play the main role, despite the fact that the acceleration of the plasma towards the channel axis is caused mainly by the Ampere force. We found that the kernel close to the channel axis is likely to be the place where the amplification in an experiment (Rocca *et al.*, 1994*a*, 1995, 1996) can take place. The kernel is the region with a diameter on the order of $\sim 1/25$ of the channel diameter uniformly filled with hot, dense plasma. The initial plasma density increases by a factor of about 200, compared to the initial plasma density. But this is not a pinch effect as, due to the lack of the electric current in the channel

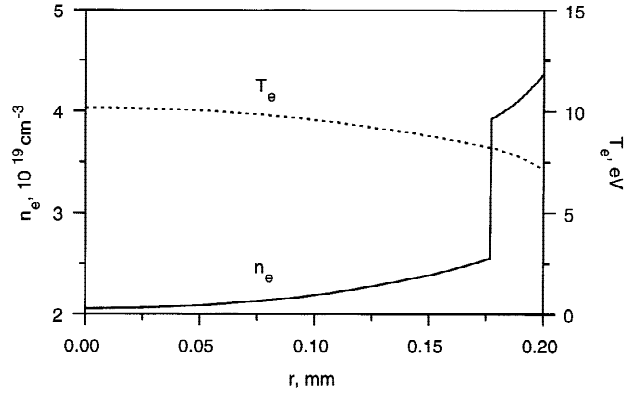

Fig. 13. Radial distribution of electron density n_e and electron temperature T_e at moment $t = 100$ ns, for the same parameters as in Figure 11.

center, electromagnetic forces do not play any role at this stage. In the absence of the current no MHD instabilities, typical of *Z*-pinches, can occur. Therefore we can conclude that the plasma behavior in the kernel can be described in the frame of hydrodynamics. The physical nature of the compression can be described in terms of the dynamics of compression flows generated by converging shock waves. The radial distributions of plasma density and temperature inside the emitting kernel are uniform. The electric current distribution inside the channel is nonuniform. A fraction of the electric current flows close to the wall and causes heating and subsequent ablation. Another fraction of the electric current is localized near the channel axis. Plasma acceleration and compression at the initial stage of the discharge are both caused by this fraction of electric current. The fraction of the electric current localized close to the wall does not take part in the plasma acceleration, but only in heating the wall. The investigation of the capillary discharge dynamics allows us to identify the formation of a plasma kernel responsible for X-ray amplification and to determine its spatial and time localization. From the set of simulations, simple scalings of electron temperature and plasma density have been obtained.

In the second regime, the capillary discharge fills in the channel with plasma of uniform density and slightly nonuniform temperature. Plasma is in a quasiequilibrium state. The Ampere force is balanced by the pressure gradient, and the Joule heating is compensated by energy losses via electron thermal conductivity and radiation. This situation is unstable against typical MHD instabilities of *Z*-pinches. The characteristic value of the plasma temperature is found in good agreement with experimental data; however it is not high enough to explain the existence of C^{5+} ions, for which recombination-pumped gain was reported by Steden and Kunze (1990) and by Shin *et al.* (1994). We assume that the existence of C^{5+} ions can be explained by the properties of the plasma implosion in an axially symmetric geometry.

In the discussion of the capillary plasma for laser pulse guiding, we investigated the dynamics of a capillary discharge using the one-dimensional MHD simulation code to achieve the discharge regime optimal for guiding of high-intensity ultrashort laser pulses.

We have revealed the discharge regime where, after a short transient process is completed, the plasma configuration reaches dynamical and thermal equilibrium. In the first stage, the fast compression, that is, the radial pinching of a plasma, and the reflection of the shock wave occur. The transient process being completed, when all MHD perturbations decay, the plasma is in dynamical and thermal quasiequilibrium. At this stage, the electric current vanishes and the Ampere force equals zero. The plasma pressure inside the channel is uniform and electron density has a parabolic profile with the minimum on the axis, where the plasma temperature is maximum.

This plasma configuration is free of MHD instabilities and therefore the small-scale plasma density fluctuations are damped. Consequently, we have shown that in the course of capillary discharge dynamics, plasma configuration optimal for the guiding of high intensity ultrashort laser pulses can be generated. We have demonstrated in a certain range of capillary discharge parameters, a laser pulse can be guided in the region whose transverse dimension is about 10 wavelengths of the laser light.

ACKNOWLEDGMENTS

We are grateful to J. Koga, K. Nakajima, I.V. Pogorelsky, T. Tajima, and A. Zigler for fruitful discussions.

REFERENCES

Askar'yan, G.A., Bulanov, S.V. & Sokolov, I.V. (1999). *Plasma Phys. Rep.* **25**, 549.

Benware, B.R., Macchietto, C.D., Moreno, C.H. & Rocca, J.J. (1998). *Phys. Rev. Lett.* **81**, 5804.

Bobrova, N.A., Bulanov, S.V., Esaulov, A.A. & Sasorov, P.V. (2000). *Plasma Phys. Rep.* **26**, 12.

Bobrova, N.A., Bulanov, S.V., Farina, D., Pozzoli, R., Razinkova, T.L., Sakai, J-I. & Sasorov, P.V. (1998*b*). *J. Phys. Soc. Jpn.* **67**, 3437.

Bobrova, N.A., Bulanov, S.V., Farina, D., Pozzoli, R., Razinkova, T.L. & Sasorov, P.V. (1998*a*). *Plasma Phys. Rep.* **24**, 3.

Bobrova, N.A., Bulanov, S.V., Razinkova, T.L. & Sasorov, P.V. (1996). *Plasma Phys. Rep.* **22**, 349.

Bobrova, N.A., Razinkova, T.L. & Sasorov, P.V. (1992). *Plasma Phys. Rep.* **18**, 269.

Bobrova, N.A. & Sasorov, P.V. (1993) *Plasma Phys. Rep.* **19**, 409.

Bogen, P. *et al.* (1968). *J. Opt. Soc. Am.* **58**, 203.

Borisov, A.B., Borovskij, A.V., Korobkin, V.V., Prokhorov, A.M., Shiriayev, O.B., Shi, X.M., Luk, T.S., Mcpheron, A., Solem, J.S., Boyer, K. & Rhodes, C.K. (1992). *Phys. Rev. Lett.* **68**, 2309.

Braginskii, S.I. (1957). *JETP* **33**, 645.

Braginskii, S.I. (1963). *Reviews of Plasma Physics*, (Leontovich, M.A., Ed.), Vol. 1, p. 18. New York: Consultants Bureau.

Bulanov, S.V., Esirkepov, T.Zh., Naumova, N.M. *et al.* (1996). *IEEE Trans. Plasma Sci.* **24**, 393.

Bulanov, S.V., Kamenets, F.F., Pegoraro, F. & Pukhov, A.M. (1994). *Phys. Lett. A* **195**, 84.

Bulanov, S.V., Kirsanov, V.I., Pegoraro, F. & Sakharov, A.S. (1993). *Laser Phys.* **6**, 1078.

Bulanov, S.V., Lontano, M. & Sasorov, P.V. (1997*b*). *Phys. Plasmas* **4**, 931.

Bulanov, S.V. & Sokolov, I.V. (1997). *Plasma Phys. Rep.* **23**, 190.

Bulanov, S.V., Vshivkov, V.A., Dudnikova, G.I., Naumova, N.M., Pegoraro, F. & Pogorelsky, I.V. (1997*a*). *Plasma Phys. Rep.* **23**, 300.

Chou, T.C., Katsouleas, T., Decker, C.D., Mori, W.B., Wurtele, J.S., Shvets, G. & Su, J.J. (1995). *Phys. Plasmas* **2**, 310.

Dufree, III, C. & Milchberg, H. (1993). *Phys. Rev. Lett.* **71**, 2409.

Dufree, III, C., Linch, J. & Milchberg, H. (1995). *Phys. Rev. E* **51**, 2368.

Dussart, R., Rosenfeld, W., Richard, N., Hong, D., Cachoncinlle, C., Fleurier, C. & Pouvesly, J.M. (1999). *X-ray*

Lasers 1998, (Kato, Y., Takuma, H. & Daido, H., Eds.), University of Berkshire, Reading: IOP.

D'YACHENKO, V.F. & IMSHENNIK, V.S. (1970). *Reviews of Plasma Physics*, (Leontovich, M.A., Ed.), Vol. 5, p. 394. New York: Consultants Bureau.

EHRLICH, Y., COHEN, C., ZIGLER, A., KRALL, J., SPRANGLE, P. & ESAREY, E. (1996). *Phys. Rev. Lett.* **77**, 4186.

ESAREY, E. *et al.* (1993). *Phys. Fluids B* **5**, 2690.

FISHER, U., JAGERM H. & LOCHTE-HOLTGREVEN, W. (1973). *Phys. Lett. B* **44**, 161.

GORBUNOV, L.M. & KIRSANOV, V.I. (1987). *Zh. Exp. Teor. Phys.* **93**, 509.

HOSOKAI, T., NAKAJIMA, M., AOKI, T., OGAWA, M. & HORIOKA, K. (1997). *Jpn. J. Appl. Phys.* **36**, 2327.

HOSOKAI, T. *et al.* (2000). *Opt. Lett.* **25**, 10.

JOSHI, C.J. & CORKUM, P.B. (1995). *Physics Today*, 36.

KATSOULEAS, T. & BINGHAM, R., (Guest Eds.) (1996). Special Issue on "Plasma Based Accelerators," *IEEE Trans. Plasma Science*, **24**.

KUNZE H.-J., KOSHELEV, K.N., STEDEN, C., USKOV, D. & WIESCHELBRINK, H.T. (1994). *Phys. Lett. A* **193**, 183.

LEE, K.T., KIM, S.H., KIM, D. & LEE, T.N. (1996). *Phys. Plasmas* **3**, 1340.

MAX, C.E., ARONS, J. & LANGDON, A.B. (1974). *Phys. Rev. Lett.* **33**, 209.

MCCORKLE, R.A. (1981). *Appl. Phys. Lett.* **26**, 261.

MCCORKLE, R.A. (1983). *Nuovo Cimento B* **77**, 31.

MODENA, A., NAJMUDIN, Z.J., DANGOR, A.E. *et al.* (1995). *Nature* **337**, 606.

MORENO, C.H., MARCONI, M.C., KANIZAY, K., ROCCA, J.J., USPENSKII, YU.A., VINOGRADOV, A.V. & PERSHIN, YU.A. (1999). *Phys. Rev. E* **60**, 911.

MORENO, C.H., MARCONI, M.C., SHLYAPTSEV, V.N., BENWARE, B.R., MACCHIETTO, J.L., CHILLA, J.L.A. & ROCCA, J.J. (1998). *Phys. Rev. A* **58**, 1509.

MORGAN, C.A., GRIEM, H.R. & ELTON, R.C. (1994). *Phys. Rev. E* **49**, 2282.

MORGAN, C.A., GRIEM, H.R. & ELTON, R.C. (1995). *Phys. Plasmas* **2**, 2847.

NAKAJIMA, K., FISHER, D., KAWAKUBO, T. *et al.* (1995). *Phys. Rev. Lett.* **74**, 4428.

NEUDACHIN, V.V. & SASOROV, P.V. (1993). *Nucl. Fusion* **33**, 475.

PEASE, R.S. (1957). *Proc. Roy. Soc.* **70**, 45.

POGORELSKY, I.V., VAN STEENBERGEN, A., FERNOW, R., KIMURA, W.D. & BULANOV, S.V. (1996). CO_2 Laser Technology for Advanced Particle Accelerators. *Proc. Seventh Workshop on Advanced Accelerator Concepts* #BNL-63649.

ROCCA, J.J. (1999). *Rev. Sci. Instrum.* **70**, 3799.

ROCCA, J.J. *et al.* (1996). *X-ray Lasers 1996*, (Svanberg, S. & Wahlström, C.-G., Eds.), p. 176. Bristol & Philadelphia: IOP.

ROCCA, J.J., BEETLE, D.C. & MARCONI, M.C. (1988). *Opt. Lett.* **13**, 565.

ROCCA, J.J., CORTAZAR, O.D., SZAPIRO, B., FLOYD, K. & TOMASEL, F.G. (1993). *Phys. Rev. E* **47**, 1299.

ROCCA, J.J., CORTAZAR, O.D., TOMASEL, F.G. & SZAPIRO, B. (1994*b*). *Phys. Rev. E* **48**, R2378.

ROCCA, J.J., SHLYAPTSEV, V., TOMASEL, F.G., CORTAZAR, O.D., HARTSHORN, D. & CHILLA, J.L.A. (1994*a*). *Phys. Rev. Lett.* **73**, 2192.

ROCCA, J.J., TOMASEL, F.G., MARCONI, M.C., SHLYAPTSEV, V., CHILLA, J.L.A., SZAPIRO, B. & GIUDICE, G. (1995). *Phys. Plasmas* **2**, 2547.

SETHIAN, J.D., GERBER, K.A. & ROBSON, A.E. (1985). *Bull. Am. Phys. S.* **30**, 1388.

SHIN, H.-J., KIM, D.-E. & LEE, T.-N. (1994). *Phys. Rev. E* **50**, 1376.

SHLYAPTSEV, V.N. *et al.* (1996). *X-ray Lasers 1996*, (Svanberg, S. & Wahlström, C.-G., Eds.), p. 215. Bristol & Philadelphia: IOP.

SPRANGLE, P. *et al.* (1988). *Appl. Phys. Lett.* **53**, 246.

SPRANGLE, P. *et al.* (1990). *Phys. Rev. A* **41**, 4463.

STANYUKOVICH, K.P. (1960). Unsteady motion of continuous media. Oxford, UK: Pergamon Press.

STEDEN, C. & KUNZE, H.-J. (1990). *Phys. Lett. A* **151**, 534.

SUN, G.Z., OTT, E., LEE, Y.C. & GUZDAR, P. (1987). *Phys. Fluids* **30**, 526.

TAJIMA, T. (1985). *Laser Part. Beams* **3**, 1432.

TAJIMA, T. & DAWSON, J.M. (1979). *Phys. Rev. Lett.* **43**, 262.

TOMASEL, F.G., ROCCA, J.J., CORTAZAR, O.D., SZAPIRO, B. & LEE, R.W. (1993). *Phys. Rev. E* **47**, 3590.

WAGNER, T., EBERL, E., FRANK, K., HARTMANN, W., HOFFMANN, D.H.H. & TKOTZ, R. (1996). *Phys. Rev. Lett.* **76**, 3124.

WAGNER, R., CHEN, S.-Y., MAKSIMCHUK, A. & UMSTADLER, D. (1997). *Phys. Rev. Lett.* **78**, 3125.

ZELDOVICH, YA.B. & RAIZER, YU.P. (1967). *Physics of Shock Waves and High-Temperature Hydrodynamic Phenomena*. New York: Academic Press.